Scattering, loss, and gain of surface plasmons

Beijnum, F. van

Citation

Beijnum, F. van. (2013, May 15). *Scattering, loss, and gain of surface plasmons. Casimir PhD Series*. Retrieved from https://hdl.handle.net/1887/20870

Cover Page

Universiteit Leiden

The handle http://hdl.handle.net/1887/20870 holds various files of this Leiden University dissertation.

Author: Beijnum, Frerik van
Title: Scattering, loss, and gain of surface plasmons
Issue Date: 2013-05-15

Rayleigh scattering of surface plasmons by a subwavelength hole extracted from wavelength dependence of speckle patterns

Rayleigh scattering of light is well known for being inversely proportional to the fourth power of the wavelength, but so far it is unclear whether this scaling also applies to the scattering of surface plasmons at a subwavelength hole. We extract the scattering cross section of a surface plasmon scattering at a single hole from the transmission of random patterns of subwavelength holes. The measured scattering cross section for surface plasmon scattering at a single hole has a stronger wavelength dependence than the traditional λ^{-4} scaling found for small particles. Although this experimentally found scaling is consistent with recent theoretical work, the magnitude of the scattering cross section is about an order of magnitude larger than predicted.

5.1 Introduction

Subwavelength holes are important building blocks for novel photonic structures, given that these holes are used in metamaterials [4, 79], photonic crystal slabs [80], sensors [29] and possibly thin film solar cells [81]. In the context of the extraordinary optical transmission [28], the transmission of light through single subwavelength holes in metal films has attracted much interest and its physics is surprisingly rich [43, 55, 82].

The excitation [10, 46] and scattering [83, 84] of surface plasmons by single subwavelength holes has been studied both theoretically and experimentally. The wavelength dependence of these scattering processes might reveal the underlying physics of surface plasmon scattering. Also, deep understanding of these scattering events is of paramount importance for recently developed microscopic models [36, 37]. So far, this wavelength dependence is only studied using metal hole arrays. One study reports the traditional [85] λ^{-4} dependence [86], while another study reports a λ^{-n} wavelength dependence where the power n depends strongly on hole size [87]. Both experimental observations contradict theories on surface plasmon scattering [83, 84].

For surface plasmons scattered at a single hole, the scattering cross section has unit length instead of an area [83, 84]. This is because the cross section is the scattered power divided by the incident power per unit width of the surface plasmon mode. This width is along the surface and perpendicular to the propagation direction [83, 84, 88]. Using the power per unit width has the advantage that it is independent of the surface plasmon mode size.

Figure 5.1: a-c, These experiments probe three scattering processes: **a,** the coupling of a surface plasmon to free space via a single hole; **b,** surface plasmon mediated transmission, where first a surface plasmon is excited at one hole and transmitted at another hole; **c,** direct transmission through a subwavelength hole. **d,** Random patterns of subwavelength holes are illuminated by a spectrally filtered supercontinuum laser source, of which we scan the wavelength. The change of the speckle pattern as a function of wavelength difference $\Delta\lambda$ is quantified by calculating the correlation $C(\Delta\lambda)$.
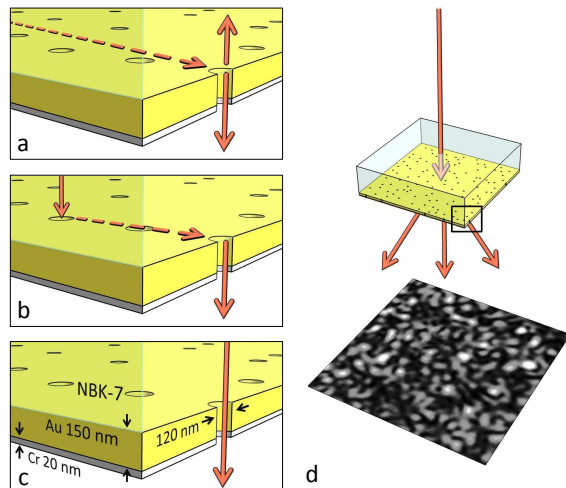
Because the scattering cross section for surface plasmons has unit length, the traditional expression [85] of a product of a volume squared and λ^{-4} can not be correct.

In this chapter we extract Rayleigh scattering of surface plasmons by single subwavelength holes from the transmission of random patterns of these holes. An important advantage of these random patterns is that most interference effects can be averaged, in contrast to the transmission of arrays which is entirely dominated by interference effects. In random patterns it is also straightforward to compare samples of different hole densities, which allows separating the ohmic and radiative losses of the surface plasmons [38].

The results presented in this chapter revolve around three quantities, of which we measure the wavelength dependence: the surface plasmon absorption length L_{abs}, the scattering cross section σ, and the intensity ratio cross section A. The surface plasmon absorption length L_{abs} contains only the ohmic loss of the surface plasmons. The scattering cross section σ characterizes the radiative loss of a surface plasmon at a single hole (Fig. 5.1a). The intensity ratio cross section A describes the transmission of light via a surface plasmon where first a surface plasmon is excited and thereafter transmitted through the hole (Fig. 5.1b). This parameter A contains a normalization to the direct transmission (Fig. 5.1c). Before presenting the wavelength dependence of L_{abs}, σ and A, we show how we extract these quantities from the transmission of random hole patterns. Our approach is discussed in more detail in ref. [38].

5.2 Experiment

Our experiments are performed on a series of random patterns of subwavelength holes in a metal film. The series contains eight patterns of which only the hole density is varied. We choose the area per hole to be qa_0^2, with $a_0 = 0.45$ μm and $q \in [1, 2, 3, 4, 9, 16, 25, 36]$. The circular holes (diameter of 120 ± 6 nm) perforate a 150 nm thick gold film which is deposited directly on glass, omitting the commonly used adhesion layer. A subsequently deposited 20 nm chromium layer damps the surface plasmons on the gold-air interface, allowing us to selectively study surface plasmons on the gold-glass interface (see Fig. 5.1c).

We illuminate these random patterns of subwavelength holes with monochromatic light and record the far field speckle intensity $I(\vec{\theta}, \lambda)$ (see Fig. 5.1d). The change of the speckle pattern with wavelengt can be quantified by calculating the correlation between the measured speckle intensity at wavelengths λ_0 and $\lambda_1 = \lambda_0 + \Delta\lambda$, resulting in a correlation function $C(\Delta\lambda)$ [66, 68, 70, 72, 89, 90]. We perform these measurements in a large wavelength range using a supercontinuum laser source (Fianum Whitelase 400SC)

Figure 5.2: The measured correlation functions $C(\Delta\lambda)$ have a wavelength-dependent contribution caused by surface plasmons propagating on the gold-glass interface, and a wavelength-independent contribution resulting from light that is directly transmitted through the holes. The correlation function depends strongly on hole density: the width increases with hole density while the background decreases. For the clarity of the figure, the plots for $\rho = 1.6$ μm^2 and $\rho = 2.5$ μm^2 are offset by -0.1 and -0.2 respectively.
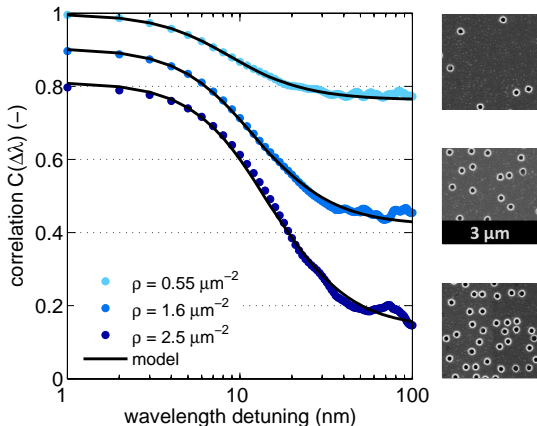
of which we select a narrow line (~ 1 nm) with a spectrometer.

Using a simple model, which assumes that only surface plasmons are excited at the holes and thus neglects the quasi-cylindrical wave contribution [35, 44, 47], we find an analytic expression for the correlation function:

$$C(\Delta\lambda) = \frac{1}{\langle I_d + I_s \rangle^2} \left| \langle I_d \rangle + \frac{\langle I_s \rangle}{1 - iL_{\text{tot}} \operatorname{Re}\left[\Delta k_{\text{spp}}\right]} \right|^2. \qquad (5.1)$$

Equation (5.1) contains two density dependent parameters: L_{tot}, the propagation distance of the surface plasmons which includes both radiative and nonradiative losses; $\langle I_s \rangle / \langle I_d \rangle$, which defines the intensity ratio between light transmitted via surface plasmons ($\langle I_s \rangle$) and directly through the holes ($\langle I_d \rangle$). The term $\operatorname{Re}\left[\Delta k_{\text{spp}}\right]$ is the difference between the surface plasmon momenta at wavelengths λ_0 and λ_1. To good approximation Eq. (5.1) is a Lorentzian with an almost wavelength independent background correlation $\langle I_d \rangle^2 / \langle I_d + I_s \rangle^2$.

Figure 5.2 shows three examples of measured correlation functions (on a log-linear scale) for three different hole densities. The scans in this plot are performed from 690 nm ($\Delta\lambda = 0$ nm) to 790 nm ($\Delta\lambda = 100$ nm). With increasing hole density the background correlation (i.e. at large $\Delta\lambda$) decreases while the spectral width of the correlation increases. The observation that the background correlation decreases shows that the efficiency of transmission via surface plasmons increases with hole density as a larger fraction of the excited surface plasmons is coupled out instead of being absorbed. This increase in outcoupling is also evidenced by the increasing spectral width, which is directly related to the losses of the surface plasmons.

The three fits in Fig. 5.2 are based on Eq. (5.1) and in good correspondence with the data. From each fit two density dependent parameters can

be extracted: L_{tot} and $\langle I_s \rangle / \langle I_d \rangle$. The density dependence of L_{tot} can be quantified in terms of two density-independent parameters:

$$L_{\text{tot}}^{-1} = L_{\text{abs}}^{-1} + \rho\sigma, \qquad (5.2)$$

where L_{abs} is the surface plasmon absorption length in the absence of the holes and σ is a scattering cross section that describes the radiative loss of a surface plasmon at a single hole (see Fig. 5.1c). Because of the two dimensional nature of our system, the hole density ρ has unit per area and the scattering cross section σ has unit length. In the appendix we show that we can fit Eq. (5.2) to the measured density dependence of L_{tot}. This fit yields two density-independent parameters that apply to all structures: the absorption length of the surface plasmons L_{abs} and the scattering cross section σ at a single hole.

The second parameter that we obtain from the correlation functions is the intensity ratio $\langle I_s \rangle / \langle I_d \rangle$. In the appendix the experimentally obtained ratios are presented as a function of hole density. Using our model, we can express this intensity ratio in terms of the hole density ρ [38]:

$$\frac{\langle I_s \rangle}{\langle I_d \rangle} = \frac{A\rho}{\rho\sigma + L_{\text{abs}}^{-1}}, \qquad (5.3)$$

where A is a third density-independent parameter: the intensity ratio cross section. Equation (5.3) fits the experimental data of the density-dependent intensity ratio, using only A as a free parameter (see appendix).

This parameter A comprises two different effects: first, the excitation of surface plasmons from free space at the glass side; second, the outcoupling to the air side (see Fig. 5.1b). The magnitude of A contains a normalization to the intensity transmitted directly through the hole (see Fig. 5.1c). The parameter A has unit length, which makes the right hand side of Eq. (5.3) dimensionless, as is the ratio on the left hand side.

To summarize, we can generalize the correlation functions $C(\Delta\lambda)$ of samples with different hole densities, using only three density-independent parameters: L_{abs}, σ and A. We measure the correlation functions for different values of the reference wavelength λ_0, allowing us to measure the wavelength dependence of the parameters L_{abs}, σ and A. In particular, we try to understand the wavelength dependence of the scattering parameters σ and A using Rayleigh scattering of surface plasmons at single holes as microscopic model.

5.3 Results

In Fig. 5.3 we show the measured wavelength dependence of L_{abs}. The absorption length increases by approximately a factor four from $L_{\text{abs}} \approx 5\,\mu$m to

$L_{\text{abs}} \approx 20$ μm, when the wavelength is increased from 650 nm to 950 nm. The data matches very well with the theory for which we use literature values of the refractive index of gold [54, 77]. This correspondence is very important as it demonstrates the validity of our approach, both qualitative and quantitative.

In Fig. 5.4 we plot the extracted value for the scattering cross section σ as a function of wavelength. This scattering cross section shows a steep decline from slightly more than 100 nm at a wavelength of 675 nm to around 15 nm at 875 nm. This decline is significantly steeper than the traditional expression for Rayleigh scattering ($\sigma \propto \lambda^{-4}$) which is indicated by the dashed line.

Recently, an analytic expression is derived for the scattering cross section of surface plasmons scattered at a subwavelength hole [84]. For surface plasmons scattered to the photon field this expression is:

$$\sigma = \xi \frac{k^4 a^6}{d_{\text{spp}}} \tag{5.4}$$

where a is the hole radius, k is the wave vector in air, and d_{spp} is the mode size of the surface plasmon, i.e. the $1/e$ width of the intensity tail into the dielectric. The dimensionless proportionality constant ξ is radius independent for $ka \ll 1$. For a hole in a perfect electrical conductor slab of zero thickness $\xi = 0.24$. Hence, the expression is essentially equivalent to that for scattering of light by three dimensional particles, with the exception that the surface plasmon mode size comes in as a proportionality factor. This factor indicates that the hole is polarized more effectively when the surface plasmon mode is more compact. The wavelength dependent mode size of a surface plasmon at a metal-air interface is $d_{\text{spp}} \approx \sqrt{|\epsilon|}/(2k)$, with ϵ the dielectric constant of the metal (assuming $|\epsilon| \gg 1$).
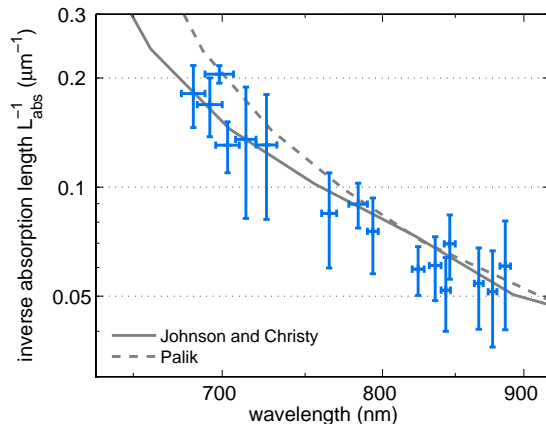

Figure 5.3: Inverse absorption length L_{abs}^{-1} as a function of wavelength, as extracted from our experiments. The obtained absorption length is in good agreement with theory showing both the validity of our experiment and the quality of the gold layer.
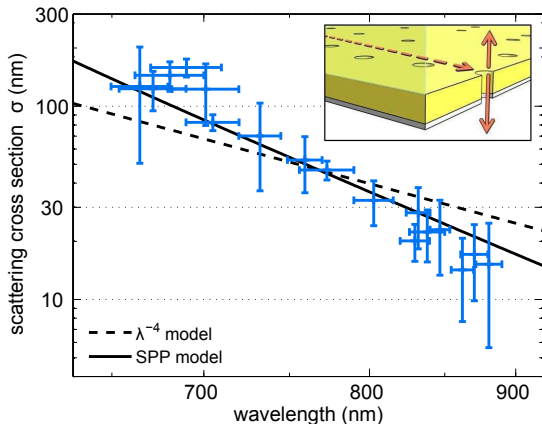
Figure 5.4: The scattering cross section σ, describing the radiative loss of a surface plasmon at a single hole, decreases almost a factor 10 in the measured wavelength range.

Fitting Eq. (5.4) to the data in Fig. 5.4, we see a much better correspondence than for $\sigma \propto \lambda^{-4}$. This is a very important result, as it shows that the wavelength dependence of the surface plasmon scattering can be understood and described well using a simple expression. The wavelength dependence of surface plasmon scattering at subwavelength holes can apparently be understood by combining Rayleigh scattering with the surface plasmon mode size.

The prefactor predicted by the theory [84] ($\xi = 0.24$) is roughly two orders of magnitude different from our results ($\xi = 63 \pm 27$), whereas the experiments published with the theory agree within a factor two [84]. The theory, however, is derived for a metal-air interface. By adapting the theory to a metal-glass interface, we find that Eq. (5.4) should be multiplied by $n^6 = 11.9$, with n the refractive index of glass (see appendix), thereby increasing the theoretical expectation to 2.8. In the appendix we speculate that the remaining order of magnitude can be explained by the field penetration into the metal, which is neglected when a perfect electrical conductor is assumed.

Given the promising results for the scattering cross section, we may also be able to understand the wavelength dependence of the intensity ratio cross section A. In Fig. 5.5 we plot the extracted value for A as a function of wavelength: A spans roughly an order of magnitude and is of comparable magnitude as σ, suggesting that A and σ may be related. Similar to σ, A has a stronger wavelength dependence than λ^{-4}.

In the appendix we derive a relation between A and σ, which is $A = \sigma \eta 3\lambda/(n16d_{spp})$. The efficiency η describes, for an incident surface plasmon, how much power is radiated to the substrate relative to the total power scattered out at this hole. The factor $3\lambda/(n16d_{spp})$ describes, for a magnetic
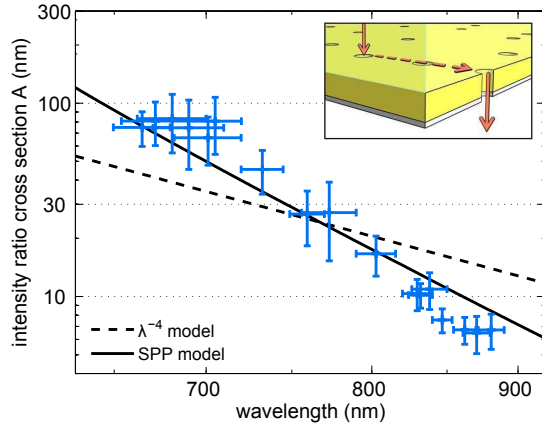
Figure 5.5: The intensity ratio cross section, A, represents transmission of light via a surface plasmon, that is excitation at one hole and transmission at another hole. This parameter also decreases almost a factor 10 in the measured wavelength range and is comparable in magnitude to the scattering cross section σ.

dipole, how much power is radiated to surface plasmons relative to the power radiated to the free space at the substrate side. This calculation assumes that both the surface plasmon excitation and outcoupling are mediated via the same (magnetic) dipole moment.

In Fig. 5.5 we plot a fit of $A = \sigma\eta 3\lambda/(n16d_{spp})$, using η as free parameter and the value of ξ we obtained from Fig. 5.4 which describes σ. We obtain a fitted value of $\eta = 0.67 \pm 0.19$, which is reasonable as we expect this efficiency to be close to, but smaller than, one. This demonstrates the consistency of the experimental data and the data analysis. We are able to relate two independent quantities (the intensity ratio and the spectral width) to the same scattering cross section σ using a simple efficiency factor.

These measurements are also performed on square holes with side length 125 ± 5 nm, showing the same wavelength dependencies for both σ and A (see appendix). For these square holes, the experimentally obtained values for ξ and η are very similar to those of circular holes.

5.4 Conclusions

The scattering cross section of surface plasmons scattered by a subwavelength hole is measured in the wavelength range of 650-900 nm. The reported wavelength dependence is stronger than Rayleigh scattering predicts, because a surface plasmon polarizes the hole less efficiently at larger wavelengths. Nonetheless, this behavior can be captured in a simple expression.

Additionally, the measured scattering cross section explains the ratio between surface plasmon mediated transmission and direct transmission of random hole patterns. Our results therefore imply that it may be viable to model particular complex plasmonic structures, like metal hole arrays, using only

physical parameters like the hole size, hole density and film thickness. However, first the magnitude of the measured scattering cross section needs to be understood as it is one order of magnitude larger than recent theoretical predictions.

The presented methodology of obtaining scattering cross sections from transmission measurements on samples of different hole densities is surprisingly powerful, and may prove to be fruitful outside plasmonics too. Moreover, we showed the advantage of using random patterns instead of arrays, as the randomness allows measurements at virtually any wavelength without changing the illumination angle and thus the character of the excited dipole moments.

Appendix

This appendix consists of four parts. We first present a derivation of the model used to fit our experimental correlation functions. Second, the parameters in our model are shown to be related the relevant magnetic and electric polarizabilities. In the third part we show the experimentally obtained density dependence of the propagation length and the intensity ratio, from which we obtained density independent parameters. In the last part, we present our results for square holes, presenting the wavelength dependence of the scattering cross section and of the intensity ratio cross section.

Model

In our experiments we calculate the correlation between two far-field speckle patterns $I(\lambda_0, \vec{\theta_0})$ and $I(\lambda_1, \vec{\theta_1})$, and express it as an experimental speckle correlation function (SCF). We have fitted the measured correlation function to a model containing two experimental parameters. In this section we show how we derived this model.

We calculate the correlation between two speckle patterns, which are both normalized to their mean intensity. Assuming the experimental correlation function is well described by an ensemble average, the correlation is expressed as follows:

$$C(\lambda_0, \lambda_1) \equiv \frac{\left\langle I(\lambda_0, \vec{\theta_0}) I(\lambda_1, \vec{\theta_1}) \right\rangle}{\left\langle I(\lambda_0, \vec{\theta_0}) \right\rangle \left\langle I(\lambda_1, \vec{\theta_1}) \right\rangle} - 1, \tag{5.5}$$

where $\langle \cdot \rangle$ denotes ensemble averaging. Using Isserlis theorem [74] Eq. (5.5) can be rewritten in terms of the electric fields $E(\lambda_0, \vec{\theta_0})$ and $E(\lambda_1, \vec{\theta_1})$, which simplifies further calculations:

$$C(\lambda_0, \lambda_1) = \frac{\left| \left\langle E(\lambda_0, \vec{\theta_0}) E^*(\lambda_1, \vec{\theta_1}) \right\rangle \right|^2}{\left\langle I(\lambda_0, \vec{\theta_0}) \right\rangle \left\langle I(\lambda_1, \vec{\theta_1}) \right\rangle}, \tag{5.6}$$

where * denotes the complex conjugate. The field at a particular angle $\vec{\theta}$, is a summation of the fields at all individual holes i multiplied by a phase factor $\exp\left[i\vec{x_i}\vec{k_{||}}(\lambda)\right]$ that depends on the position of the hole $\vec{x_i}$, where $\left|\vec{k_{||}}(\lambda_0)\right| = (2\pi/\lambda)\sin\left|\vec{\theta}\right|$. Hence the total field $E(\lambda, \vec{\theta})$ is:

$$E(\lambda, \vec{\theta}) = \sum_i E_i(\lambda) \exp\left[i\vec{x_i}\vec{k_{||}}(\lambda)\right], \tag{5.7}$$

Inserting Eq. (5.7) into Eq. (5.6) results in a double summation (over i and i') of which the terms with $i \neq i'$ have an ensemble average of zero. For the terms with $i = i'$ we find $\left\langle E_i(\lambda_0) E_i^*(\lambda_1) \exp\left[ix_i(\vec{k}_{||}(\lambda_0) - \vec{k}_{||}(\lambda_1))\right]\right\rangle$. This reduces to $\langle E_i(\lambda_0) E_i^*(\lambda_1)\rangle$ if we choose $\vec{k}_{||}(\lambda_0) = \vec{k}_{||}(\lambda_1)$. This condition can be achieved experimentally by rescaling the recorded images [38]. Hence our expression for the correlation function is now:

$$C(\lambda_0, \lambda_1) = \frac{\left|\langle E_i(\lambda_0) E_i^*(\lambda_1)\rangle\right|^2}{\langle I_i(\lambda_0)\rangle\langle I_i(\lambda_1)\rangle}, \tag{5.8}$$

This expression shows that we only have to consider the field at a single hole i, because the ensemble-averaged contribution of each hole is identical. Therefore we will now continue to derive an expression for the field at a single hole. We assume that this field has two contributions: a directly transmitted field $E_{d,i}(\lambda)$ and a surface plasmon field $E_{s,i}(\lambda)$, thereby neglecting the possible influence of the quasi-cylindrical wave [35, 44, 47] which is found at distances of roughly a wavelength from the hole. Inserting $E_i(\lambda) = E_{d,i}(\lambda) + E_{s,i}(\lambda)$ into Eq. (5.8) we obtain:

$$C \propto \left|\langle E_{d,i}(\lambda_0) E_{d,i}^*(\lambda_1)\rangle + \langle E_{s,i}(\lambda_0) E_{s,i}^*(\lambda_1)\rangle\right|^2. \tag{5.9}$$

To find this expression we use $\left\langle E_{d,i}^*(\lambda_1) E_{s,i}(\lambda_0) + E_{d,i}(\lambda_0) E_{s,i}^*(\lambda_1)\right\rangle = 0$, resulting from the random phase of the surface plasmon field.

We can specify $E_{s,i}(\lambda)$ further, assuming that the surface plasmons are radiated with an angular dependence $A_0(\lambda, \phi_j)$ from another hole j. These surface plasmons decay as a cylindrical wave $(1/\sqrt{r_{ij}})$ combined with an exponential decay due to radiative and nonradiative losses, given by the following expression:

$$E_{s,i}(\lambda) = \sum_j \frac{A_0(\lambda, \phi_j)}{\sqrt{r_{ij}}} \exp\left[-\frac{1}{2}L_{\text{tot}}^{-1}(\lambda) r_{ij} + i\operatorname{Re} k_{\text{spp}}(\lambda) r_{ij}\right], \tag{5.10}$$

with $L_{\text{tot}}^{-1}(\lambda) = \rho\sigma(\lambda) + 2\operatorname{Im} k_{\text{spp}}(\lambda)$ the total propagation length, which has a contribution from radiative decay $(\rho\sigma)$ and absorption $L_{\text{abs}}^{-1} = 2\operatorname{Im} k_{\text{spp}}(\lambda)$. Please note that the amplitude cross section used in previous work [38] is a factor two smaller than the (more common) intensity cross section used here. If we calculating the product $E_{s,i}(\lambda_0) E_{s,i}^*(\lambda_1)$ we find:

$$E_{s,i}(\lambda_0) E_{s,i}^*(\lambda_1) = \sum_j \frac{A_0(\lambda_0, \phi_j) A_0^*(\lambda_1, \phi_j)}{r_{ij}} \times \tag{5.11}$$

$$\exp\left[-\frac{1}{2}(L_{\text{tot}}^{-1}(\lambda_0) + L_{\text{tot}}^{-1}(\lambda_1)) r_{ij} + i\operatorname{Re}[\Delta k_{\text{spp}}] r_{ij}\right],$$

where:

$$\mathrm{Re}\left[\Delta k_{\mathrm{spp}}\right] = \mathrm{Re}\, k_{\mathrm{spp}}(\lambda_0) - \mathrm{Re}\, k_{\mathrm{spp}}(\lambda_1) = \frac{2\pi}{\lambda_0\lambda_1}\left(\Delta\lambda n_{\mathrm{eff}}(\lambda_0) - \Delta n_{\mathrm{eff}}\lambda_1\right)$$
(5.12)

with $\Delta\lambda = \lambda_1 - \lambda_0$ and $\Delta n_{\mathrm{eff}} = n_{\mathrm{eff}}(\lambda_1) - n_{\mathrm{eff}}(\lambda_0)$. For $\Delta n\lambda_0 << \Delta\lambda n_{\mathrm{eff}}(\lambda_0)$ this is expressed as:

$$\mathrm{Re}\, k_{\mathrm{spp}}(\lambda_0) - \mathrm{Re}\, k_{\mathrm{spp}}(\lambda_1) = 2\pi\left(\frac{\Delta\lambda n_{\mathrm{eff}}(\lambda_0)}{\lambda_0\lambda_1}\right)$$
(5.13)

In case of an ensemble average, we can replace the summation in Eq. (5.12) with an integral using the average number of holes in an infinitesimal area: $\rho r dr d\phi$. This integral over a complex exponential results in what is essentially a complex Lorentzian. The resulting correlation function is:

$$C = \frac{1}{\langle I_d + I_s\rangle^2}\left|\langle I_d\rangle + \frac{\langle I_s\rangle}{1 - iL_{\mathrm{tot}}\,\mathrm{Re}\left[\Delta k_{\mathrm{spp}}\right]}\right|^2,$$
(5.14)

where:

$$L_{\mathrm{tot}}^{-1} = \frac{1}{2}(L_{\mathrm{tot}}^{-1}(\lambda_0) + L_{\mathrm{tot}}^{-1}(\lambda_1)),$$
(5.15)

$$\langle I_d\rangle = \langle E_d(\lambda_0)E_d^*(\lambda_1)\rangle,$$
(5.16)

$$\langle I_s\rangle = \rho L_{\mathrm{tot}}\langle A_0(\lambda_0,\phi)A_0^*(\lambda_1,\phi)\rangle_\phi,$$
(5.17)

where $\langle\cdot\rangle_\phi = \int_0^{2\pi}\langle\cdot\rangle\, d\phi$. The factor A in the main manuscript is:

$$A \equiv \frac{\langle A_0(\lambda_0,\phi)A_0^*(\lambda_1,\phi)\rangle_\phi}{\langle E_d(\lambda_0)E_d^*(\lambda_1)\rangle} = \frac{\langle I_s\rangle}{\langle I_d\rangle}(\rho L_{\mathrm{tot}})^{-1}.$$
(5.18)

To fit Eq. (5.14) we assume that $\langle I_d\rangle/\langle I_s\rangle$ and L_{tot} are wavelength independent within the scan range. Hence these fitted values are an average value over the wavelength range of interest. In the main manuscript it is shown that, although some approximations had to be made, the fit function works very well.

Relating model parameters to polarizability

Recent work has calculated the scattering cross section of the hole in terms of its polarizability [84]. This work shows that there are two relevant dipole moments in the surface plasmon scattering problem: a electric dipole oriented normal to the surface and a magnetic dipole oriented parallel to the surface.

In this section we will briefly discuss this calculation, trying to clarify the assumptions made. Hereafter we will try to relate the calculated scattering cross section to the intensity ratio cross section A extracted from our measurements.

The calculation assumes a surface plasmon on a metal dielectric interface, of which the power per length $P/L_\perp$ is calculated, analogous to the intensity in three dimensions. Using the induced dipole moments, the authors calculate the power radiated to free space P_{out} and to the surface plasmon field P_{spp}. When calculating this radiation, a closed film (i.e. without a hole) is assumed.

By dividing these radiated powers by $P/L_\perp$ a scattering cross section can be calculated for the scattering to free space (σ) and the scattering to surface plasmons (σ_{spp}) [84]:

$$\sigma = \frac{P_{out}}{P/L_\perp} \approx \frac{32\pi k_0^5}{3\sqrt{|\epsilon|}}(|\alpha_E|^2 + |\alpha_M|^2) \tag{5.19}$$

$$\sigma_{spp} = \frac{P_{spp}}{P/L_\perp} \approx \frac{8\pi^2 k_0^5}{|\epsilon|}(2|\alpha_E|^2 + |\alpha_M|^2) \tag{5.20}$$

Strikingly, both expressions have a different dependence on the dielectric constant ϵ of the metal. Our understanding of this is as follows: the magnitude of the dipole moment induced by an incident surface plasmon is inversely proportional to the mode size $d_{spp} \approx \sqrt{|\epsilon|}/(2k_0)$. The radiation to free space is comparable to that of a normal dipole, that is it has no dependency on ϵ. Radiation to the surface plasmon field, however, scales with the width of the angular spectrum [91] of the surface plasmon. This width is proportional to λ/d_{spp}, yielding an extra factor $\propto 1/\sqrt{|\epsilon|}$.

Expressing the equations in terms of d_{spp} and λ/d_{spp} yields:

$$\sigma \approx \frac{1}{d_{spp}}(16/3)\pi k_0^4 \left(|\alpha_E|^2 + |\alpha_M|^2\right) \tag{5.21}$$

$$\sigma_{spp} \approx \frac{\lambda}{d_{spp}^2}\pi k_0^4 \left(2|\alpha_E|^2 + |\alpha_M|^2\right) \tag{5.22}$$

where the factor $(16\pi/3)\left(|\alpha_E|^2 + |\alpha_M|^2\right)$ is what we call η in the main manuscript. If the electric polarizability is negligible, the ratio between these two cross sections is $\sigma_{spp}/\sigma = 3\lambda/(16 d_{spp}) \approx 0.5$, for gold at 800 nm. This ratio is the power radiated to the surface plasmon field relative to that of the free space modes for a magnetic dipole. The same ratio can also be found by comparing the density of modes of the surface plasmon field to that of free space modes.

The theory in ref. [84] assumes that the surface plasmon is on a metal-air interface. In our experiment, however, it is a gold-glass interface, which

has some consequences for the quantitative agreement between the theory and experiment. For Rayleigh scattering, the expression is in terms of the wave vector inside the medium [92] ($k = n2\pi/\lambda$), hence we expect k_0^4 has to be replaced by k^4. Additionally, $d_{spp} \approx \sqrt{\epsilon}/(2n^2 k_0)$, contains the refractive index squared and the λ in the expression $\sigma_{spp}/\sigma = 3\lambda/(16d_{spp})$ should be λ/n. The modifications together yield an increase of n^6 of the scattering cross section σ.

A last step in calculating σ is finding the appropriate values for α_M and α_E. Rotenberg *et al.* calculated these values using a hole in a perfect electric conductor. In this paper, the calculated polarizability per cubed radius a^3 is plotted as a function of the size parameter a/λ. For $a/\lambda \ll 1$ the polarizability per cubed radius is constant. For the magnetic polarizability a shape resonance is found at $a/\lambda \approx 0.2$, and for larger a/λ the polarizability per cubed radius decreases. The polarizability depends on the film thickness: a 42% increase is found comparing a infinitely thick film with a zero thickness film. For the calculations in the main manuscript, we use the zero thickness value of $\alpha_M = 0.106a^3$ and $\alpha_E = 0.054a^3$.

Using these values for the polarizability the measured scattering cross section roughly an order of magnitude larger than predicted. To explain this difference between the theory and the experiment, we consider the penetration of the optical field into the metal. This penetration is neglected in calculating the polarizability of the hole, as it is calculated assuming a perfect electrical conductor. This penetration depth (~ 25 nm) is small compared to most holes in previous experiments ($a = 25$ nm $- 500$ nm) [84], where a good agreement between theory and experiment is reported. Somewhat speculatively, we estimate the effect of the penetration depth on the polarizability by modeling a hole in a metal of finite conductivity as a hole in a perfect electrical conductor whose radius is increased with the penetration depth of the field. If this approximation is valid, this would increase the expected value of ξ by a factor $(85/60)^6 = 8.1$ to $\eta = 23 \pm 10$. This would reduce the difference between theory and experiment to a factor 2.7 ± 1.2.

Finally, we wish to relate the intensity ratio cross section A to the scattering cross section σ. In the main text we showed that the ratio A/σ is the maximum ratio between surface plasmon mediated transmission and directly transmitted light as $\langle I_s \rangle / \langle I_d \rangle \approx A/\sigma$ in the limit of high hole density. In this limit, the power flow simplifies as all excited surface plasmons are coupled out before they can be absorbed.

The power flow in the high density limit is sketched in Fig. 5.6. We assume an incident plane wave with power P_{in} which polarizes a hole and thereafter
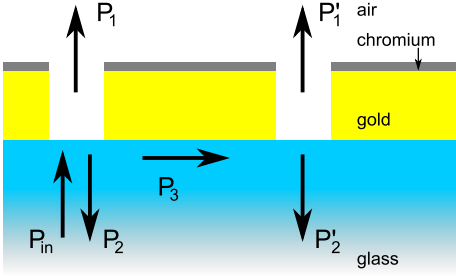
Figure 5.6: A sketch of the power flow, in the limit of high hole densities. An incident plane wave with power P_{in} induces a dipole moment. This dipole radiates into three channels: through the hole (P_1), into the substrate (P_2) and to a surface plasmon mode P_3. For high densities there is no absorption loss, and hence all power in the surface plasmon mode is scattered out at other holes. At these holes the ratio between light scattered through the hole and into the substrate is defined to be P_1'/P_2'.

radiates into three channels: P_1 through the hole, P_2 back into the substrate and P_3 into the surface plasmon field. In the high hole density limit the entire surface plasmon field is eventually scattered out, either through the hole (P_1') or back into the substrate (P_2'), such that $P_3 = P_1' + P_2'$.

The transmission via surface plasmons P_s is equal to P_1', but expressing it as $P_s = P_3 P_1'/(P_1' + P_2')$ will prove to be more useful. Given that the directly transmitted power P_d is equal to P_1, we find:

$$\frac{P_s}{P_d} = \frac{P_3}{P_2} \frac{P_2'}{P_1' + P_2'} = \eta \frac{P_3}{P_2}. \tag{5.23}$$

where we assume $P_1'/P_2' = P_1/P_2$, which physically means that the excitation and outcoupling are mediated via the same (magnetic) dipole moment. Note that we also introduced a efficiency $\eta = P_2'/(P_1' + P_2')$, which quantifies how much of the outcoupling is to the substrate relative to all light scattered out. At this point it is importantly to realize that ratio P_3/P_2 is equal to the ratio $P_{spp}/P_{out} = \sigma_{spp}/\sigma$ calculated in ref. [84]. Hence, $P_3/P_2 = \sigma_{spp}/\sigma = 3\lambda/(16nd_{spp})$. This allows us to relate A to σ:

$$\frac{A}{\sigma} = \frac{P_s}{P_d} = \eta \frac{\sigma_{spp}}{\sigma} = \eta \frac{3}{16d_{spp}} \frac{\lambda}{n}. \tag{5.24}$$

This is a very important result as we now found that the entire experiment can be described using a single scattering cross section σ, an efficiency η and some known prefactors. We expect η to be smaller but close to one, yielding a fairly accurate prediction for the relation between A and σ. This efficiency η, which has not been studied yet, basically quantifies how efficiently power is radiated to the substrate relative to the total radiative loss.

Density dependence of the loss and the intensity ratio

In this section we present the density dependence of L_{tot} and $\langle I_s \rangle / \langle I_d \rangle$ for three wavelength ranges: 705 ± 15 nm, 803 ± 13 nm and 881 ± 9 nm. We show that the measured dependencies are the same as those expected and presented in the main manuscript. Also, we show that these plots clearly reveal the strong wavelength dependence of $L_{\mathrm{abs}}(\lambda)$, $\sigma(\lambda)$, and $A(\lambda)$ presented in the main text.

In Fig. 5.7a the fit parameter L_{tot} is plotted as a function of hole density for three different wavelengths. First, it is important that the expected density dependence ($L_{\mathrm{tot}}^{-1} = L_{\mathrm{abs}}^{-1} + \rho\sigma$) is satisfied, which is the case. Second, we can see that the inverse propagation length is not only density dependent, but also wavelength dependent. The slope σ decreases from 705 ± 15 nm to 803 ± 13 nm by a factor four, and the slope almost vanishes at 881 ± 9 nm. Third, the axis cutoff that resembles the surface plasmon absorption loss, decreases with wavelength by more than a factor two. This is consistent with the theoretically expected dependence.

In Fig. 5.7b we show the density dependence of the intensity ratio $\langle I_s \rangle / \langle I_d \rangle$. The data for each wavelength shows the expected dependence ($\langle I_s \rangle / \langle I_d \rangle = A\rho L_{\mathrm{tot}}$), which is plotted as a solid line with only the vertical scale A as a free parameter. For this fit we use the values of L_{abs} and σ that we obtained for each wavelength in Fig. 5.7a to describe L_{tot}: $L_{\mathrm{tot}}^{-1} = L_{\mathrm{abs}}^{-1} + \rho\sigma$.

To relate Fig. 5.7b to the presented values for A in the main manuscript, we compare the three curves in Fig. 5.7 at low densities. There is a factor four difference between the top curve ($\lambda = 705$) and the lowest curve ($\lambda = $
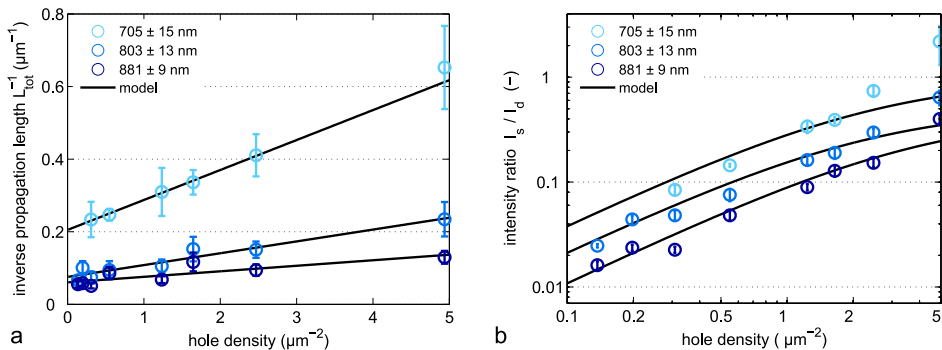

Figure 5.7: a, The inverse propagation length L_{tot}^{-1} as a function of hole density for three different wavelength ranges. Both the axis cutoff, i.e. the absorption, and the slope decrease with wavelength. **b,** The density dependence of the intensity ratio $\langle I_s \rangle / \langle I_d \rangle$. For each hole density the intensity ratio decreases with wavelength. In the low density regime the intensity ratio increases linearly.
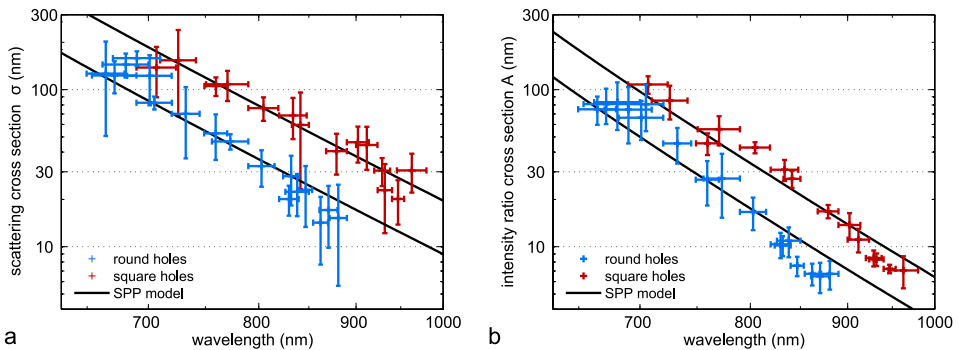
Figure 5.8: a, The measured values of the scattering cross section σ for circular and square holes. For both types the predicted wavelength dependence reproduces the data accurately. The prefactor for the round holes is smaller however. **b,** The measured values of the intensity ratio cross section A for round and square holes. Also for this parameter the predicted wavelength dependence describes the data of both round and square holes.

881). The propagation length, which is dominated by absorption at these low densities, increase roughly a factor two in this wavelength range. Hence the factor four difference between the curves in Fig. 5.7b resembles the order of magnitude change of A presented in Fig. 5.5.

Last, we note that the ratio $\langle I_s \rangle / \langle I_d \rangle$ shows an outlier at the highest hole density for each wavelength, which is systematically larger than the fitted model. These outliers are expected because we neglected the influence the quasi-cylindrical waves [35, 44, 47] in our model. Additionally, our model neglects the heavily damped surface plasmons on the gold-air interface, which is also not valid from high densities. For these reasons, these outliers are not used to obtain the fitted value for A.

Analysis of square holes

In addition to the round holes presented in the main text, we have also studied square holes. These square holes have a rib size $(125 \pm 5$ nm) slightly larger than the diameter of the round holes $(120 \pm 6$ nm). We are interested whether the shape has any influence on the magnitude of the scattering cross section its wavelength dependence.

In Fig. 5.8a we plot the results for the scattering cross section of the square holes, along with the results for round holes presented in the main text. The measured scattering cross section σ is larger for the square hole than that of the round holes, but its wavelength dependence is very similar. The suggested wavelength dependence $\sigma = \xi k^4 a^6 / d_{spp}$ accurately fits the experimental data, where we choose a the rib length divided by two. The prefactor ξ is found to

be 1.7 ± 1.3 larger for the square holes, where the large error bar is mostly the result of the error in the hole size.

In Fig. 5.8b we plot the results for the intensity ratio cross section, also with the results of the round holes. The value of A is larger for the square holes too. We fit the expected wavelength dependence of $A = 3\eta\lambda\sigma/(16nd_{spp})$, using the value of ξ just found and leaving only η as a free parameter. We find $\eta = 0.60 \pm 0.13$, which is comparable to that of round holes.

In conclusion, the data for the square hole shows the same wavelength dependence of σ and A. The prefactors η and ξ obtained for the square holes do not differ significantly from those found for round holes.